

Mechanistic Aspects of Pyrite Oxidation in an Oxidizing Gaseous Environment: An in Situ HATR–IR Isotope Study

COURTNEY R. USHER,^{*,†}
 KRISTIAN W. PAUL,[‡]
 JAYAKUMAR NARAYANSAMY,^{§,||}
 JAMES D. KUBICKI,^{§,||}
 DONALD L. SPARKS,[‡]
 MARTIN A. A. SCHOONEN,^{||,⊥} AND
 DANIEL R. STRONGIN^{*,†,||}

Department of Chemistry, Temple University, 1901 North 13th Street, Philadelphia, Pennsylvania 19122, Department of Plant and Soil Sciences, University of Delaware, 152 Townsend Hall, Newark, Delaware 19716, Department of Geosciences, The Pennsylvania State University, 308 Deike Building, University Park, Pennsylvania 16802, Department of Geosciences, Stony Brook University, Stony Brook, New York 11794, and Center for Environmental Molecular Science, Stony Brook University, Stony Brook, New York 11794-2100

The reaction of FeS₂ (pyrite) with gaseous H₂O, O₂, and H₂O/O₂ was investigated using horizontal attenuated total reflection Fourier transform infrared spectroscopy (HATR-FTIR). Spectra were interpreted with the aid of hybrid molecular orbital/density functional theory calculations of sulfate-iron hydroxide clusters. Reaction of pyrite in gaseous H₂O led primarily to the formation of iron hydroxide on pyrite. Exposure of the pyrite to gaseous O₂ after exposure to H₂O vapor led to the formation of sulfur oxyanions that included SO₄²⁻. Isotopic labeling experiments showed that after this exposure sequence the oxygen in the sulfate product was primarily derived from the H₂O reactant. If, however, pyrite was exposed to gaseous O₂ prior to pure H₂O vapor, both SO₄²⁻ and iron oxyhydroxide became significant products. Isotopic labeling experiments using the O₂-then-H₂O sequence showed that the oxygen in the SO₄²⁻ product was derived from both H₂O and O₂. The results indicate that H₂O and O₂ exhibit a competitive adsorption on pyrite, with H₂O blocking surface sites for O₂ adsorption. The extent of oxygen incorporation from either the H₂O or the O₂ component into the surface-bound sulfur oxyanion product appears to be a strong function of the relative concentration ratio of the reactant H₂O and O₂.

* To whom correspondence should be addressed. Telephone: (215) 204-7119 (D.R.S.); (215) 204-7133 (C.R.U.). Fax: (215) 204-7133 (D.R.S.). E-mail: dstrongi@temple.edu; crusher@temple.edu.

[†] Temple University.

[‡] University of Delaware.

[§] The Pennsylvania State University.

^{||} Center for Environmental Molecular Science, Stony Brook University.

[⊥] Department of Geosciences, Stony Brook University.

Introduction

A considerable number of studies have been undertaken with the aim to understand the oxidation of pyrite in detail. Much of this research is driven by the notion that a full understanding of the elementary steps of this process can lead to new strategies to inhibit its oxidation in the environment. The oxidation of pyrite in the aqueous phase leads to the formation of iron oxyhydroxides and sulfur oxyanions, chiefly sulfate (1). In the reaction steps that lead to the formation of sulfate, large amounts of protons are released. The production of acidity as a result of the exposure of pyrite to molecular oxygen and water leads to widespread occurrences of acid wastewaters near coal mines, metal mines, and other areas with pyritic rock exposed. Acid wastewater with high metal content, often referred to as acid mine drainage (AMD), impacts water quality and ecosystems in and around many active and abandoned mines (2–13). The oxidation of pyrite is also interesting on a fundamental level. Pyrite is a semiconductor material with a band gap less than 1 eV. Pyrite has been shown to be able to accept electrons and facilitate electron-transfer reactions (14). The reaction pathway or pathways that transform pyrite to its oxidation products must involve numerous elementary steps, considering that disulfide S(–I) ends up as S(VI) in the sulfate product. The nature of these elementary steps might also change depending on the redox state of the environment.

A valuable strategy to clarify some of the microscopic details of pyrite oxidation is through isotopic labeling experiments. Determining the ultimate fate, for example, of the oxygen in the water and molecular oxygen reactants gives clues to the elementary steps that determine the reaction stoichiometry. This strategy is not a new one and has been exploited to varying extents in prior research using ex situ and in situ techniques. For example, prior studies using this strategy have shown that the sulfate product is derived primarily from the water reactant when molecular oxygen is the oxidant of pyrite (1, 15–17). In these earlier studies, it is noteworthy that a small fraction of oxygen atoms in sulfate is derived from the molecular oxygen reactant, rather than water. Furthermore, recent research by our group has shown that the iron oxyhydroxide product is derived in large part from the molecular oxygen component (1).

Several different models have been proposed for the oxidation of pyrite with molecular oxygen as the reactant. A recent electrochemical model considers pyrite oxidation in solution as an electron-transfer reaction in an electrochemical cell with sulfur and iron acting as the anode (sulfur oxidation) and cathode (molecular oxygen reduction), respectively (18). The crux of this model is that sulfur and iron on the pyrite surface undergo separate reactions, a notion consistent with the fact that the activation energy for the reaction differs when either sulfate release or iron release is used as a reaction progress variable (19). While it is appealing in its simplicity to treat the reactions at the anodic and cathodic sites as independent reactions, this model does not explain how some of the oxygen in sulfate is derived from molecular oxygen. The incorporation of molecular oxygen into the sulfate product suggests that there is an additional level of complexity not considered in the electrochemical model or any of the other prior models. It is hypothesized here that the relative amount of O₂- and H₂O-derived oxygen in the sulfate product will be highly dependent on the relative ratios of the reactant concentrations. By studying pyrite oxidation under conditions with different ratios of H₂O-to-O₂ exposure it is possible to test this hypothesis. Earlier work on pyrite oxidation by pure oxygen gas (20) corroborates the notion that this reactant

TABLE 1. Calculated Frequencies for the Species Shown in Figure 1 and H-Bonded Sulfate (Not Shown)

	bidentate bridging bisulfate	monodentate bisulfate	bidentate bridging sulfate	monodentate sulfate	H-bonded sulfate
¹⁶ O	1188; 1106; 1074; 972	1204 ^a ; 1150; 1058; 955 ^a	1098; 1033; 991; 948; 900 (weak)	1171; 1090; 929; 831	1112; 1084; 1018; 938; 865
¹⁸ O	1170; 1077; 1052; 930	1167; 1125; 1022; 921	1066; 1005; 978; 938; 850	1137; 1048 ^a ; 888; 791	

^a Intensity weighted mean of two identical and closely spaced normal modes.

can be a source of the oxygen in sulfate, indicating that the two reactions on the anodic and cathodic sites may not be entirely independent.

Research detailed in the present contribution investigates the oxidation of pyrite in gaseous O₂, H₂O vapor, sequential exposures to these two reactants, and simultaneous exposure to the two reactants. In particular, the experiments use HATR-FTIR and isotopic labeling techniques to determine the partitioning of O₂- and H₂O-derived oxygen in the sulfate and iron oxyhydroxide products as a function of the relative concentration of O₂ and H₂O reactants in the gas phase. Analysis of the pyrite oxidation reaction with gaseous reactants also allows us to simplify the reaction steps that lead to the appearance of iron oxyhydroxide on the pyrite surface. While an adsorbed water layer may have a role in the formation of the iron product on the surface (transport and solvation in, precipitation from), the complication due to the possibility that the iron oxyhydroxide precipitates from solution in prior aqueous-phase research of pyrite oxidation may be eliminated. The results will show that the oxygen partitioning in the sulfate product is a sensitive function of the gaseous concentration ratio of O₂ and H₂O and on the pretreatment of the pyrite surface. For example, the isotopic distribution of the sulfate product is different if the pyrite is exposed to water vapor prior to O₂ introduction than if it is exposed to oxygen before the introduction of water into the gaseous reactant stream. In contrast to the sulfate product, the relative amount of H₂O- and O₂-derived oxygen in the iron oxyhydroxide product is insensitive to the concentration of reactant species.

Experimental Methods

Pyrite samples used for all experiments were prepared under a nitrogen (99.999% purity) atmosphere and involved cleaning approximately 0.05 g of crushed FeS₂ (from Huanzala, Peru; particle size < 75 μm) through shaking 2 min in 1 mL of 1 M HCl. This cleaning procedure was repeated five times with fresh acid, before rinsing the particles with deoxygenated water. A slurry of the pyrite particles in 0.5 mL of deoxygenated water was dispersed on a Ge HATR element in a stainless steel crystal holder (Pike Technologies) and allowed to dry under a gentle stream of nitrogen to produce an even, thin coating of pyrite particles on the crystal surface. When the sample had dried, the HATR cell was sealed with a Teflon-coated lid and placed into the infrared spectrometer.

Horizontal attenuated total reflectance infrared spectroscopic measurements were performed in a Nicolet Magna-IR 560 spectrometer using a liquid nitrogen-cooled MCT-A detector and a Pike Technologies HATR-IR base plate mounted in the IR beam path, supporting the HATR crystal plate. Single-beam spectra were recorded through 1000 scans at 4 cm⁻¹ resolution over the range 650–4000 cm⁻¹. An initial spectrum scanned at time zero (initial introduction of gas-phase reactants) was typically used as a reference for subsequent single-beam spectra to obtain absorbance spectra, which were collected over several hours to monitor changes on the pyrite surface.

Two ports are available in the Teflon-coated lid of the HATR crystal plate. For experiments in which water vapor

alone was used, prepurified N₂ gas (99.998% minimum purity) was bubbled at the rate of 2–3 bubbles/s through approximately 2 mL of deoxygenated water in a small closed vial and flowed over the sample through the ports of the HATR cell. For experiments using only molecular oxygen as the reactant, ¹⁶O₂ gas (99.997% minimum purity) was flowed through the ports. Experiments using both water vapor and O₂ gas were performed such that the O₂ gas did not bubble into the water but swept through the headspace and into the HATR cell. The flow rate of the gas in these experiments was approximately the same as that for the case where it was bubbled through the liquid. Experiments in this case were done both with water at room temperature and with water kept at ice temperature to decrease the vapor pressure of water in the vial (4.58 Torr at 0 °C vs 23.76 Torr at 25 °C). These two experimental conditions allowed us to individually flow gas streams over the pyrite that had two different H₂O-to-O₂ concentration ratios to investigate how this experimental variable affected pyrite oxidation. The exact ratios of water to oxygen were not quantified; the difference in the amount of water was controlled only by decreasing the vapor pressure of water so there would be less in the headspace to be swept into the reaction cell. We will refer to these two conditions in subsequent sections as the high and low H₂O/O₂ circumstances. Experiments were performed using H₂¹⁶O or H₂¹⁸O (Stable Isotopes, Inc., 95% ¹⁸O isotopic purity).

Theoretical calculations were performed using the electronic structure program Gaussian 03 (21), and normal modes were analyzed in GaussView 3.0. The unrestricted hybrid density functional method was employed using Becke's three-parameter nonlocal-exchange functional (22, 23) with the gradient-corrected correlation functional of Lee–Yang–Parr (24) (UB3LYP). The standard 6-31+G(d) all-electron split valence basis set including polarization and diffuse functions on all heavy atoms (non-hydrogen) was utilized. Minima on the potential energy surfaces were located from a geometry optimization calculation on the entire system where no symmetry or geometrical constraints were allowed. Frequency calculations were subsequently performed on the geometry optimized structures corresponding to stationary points on the potential energy surface to verify that a minimum was successfully located (i.e., no imaginary frequencies) and to obtain predicted IR frequencies comparable to experimental HATR-FTIR spectra. Isotopic substitution of ¹⁸O for ¹⁶O for the O atoms in the sulfate groups was performed and the frequencies were calculated for comparison against the observed isotopic frequency shifts. The calculated values are shown in Table 1 for species shown in Figure 1 as well as for sulfate in an H-bonded configuration (not shown). All calculated values were scaled by a factor of 0.9613 to account for anharmonicity and incomplete electron correlation (25, 26). In general the calculated values were in good agreement (within 5%) of experimental values. The structures used for the calculations are shown in Figure 1. Note that four H₂O molecules were included to H-bond with the model surface sulfate group to obtain results more comparable to experiment.

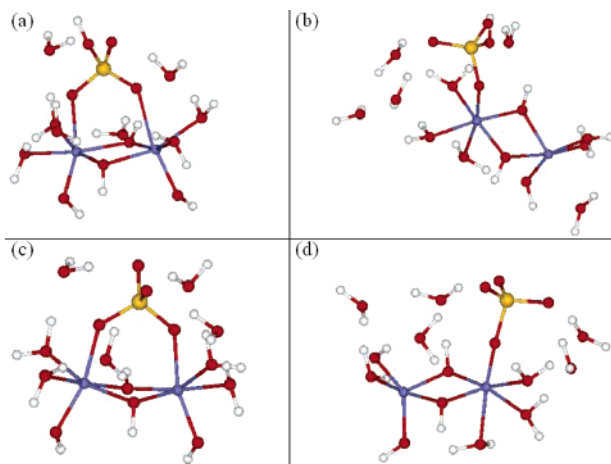


FIGURE 1. Structures used to calculate S–O vibrations on an iron oxide surface with both ^{16}O and ^{18}O : (a) bidentate bridging bisulfate (HSO_4^-); (b) monodentate bisulfate (HSO_4^-); (c) bidentate bridging sulfate (SO_4^{2-}); (d) monodentate sulfate (SO_4^{2-}). Atoms colored red are oxygen; white are hydrogen; blue, iron; yellow, sulfur.

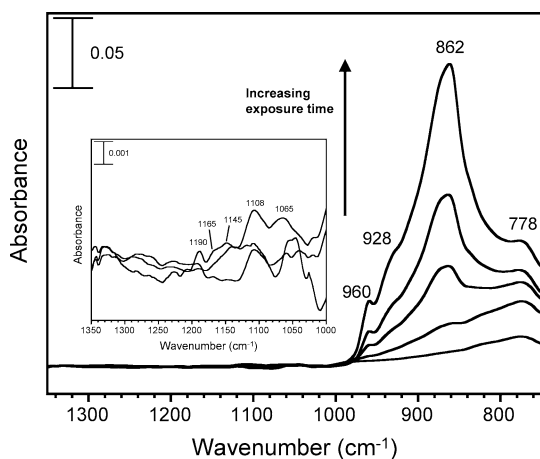


FIGURE 2. Spectra recorded as a function of time of pyrite particles exposed to a high $\text{H}_2^{18}\text{O}/\text{O}_2$ gaseous mixture (see Experimental Methods for conditions) for up to 260 min. The inset is an expansion of the spectral region $1000\text{--}1350\text{ cm}^{-1}$; for clarity only three spectra are shown (at $t = 60, 120,$ and 230 min).

Results

O_2 and Water Vapor Mixture. Figure 2 exhibits spectra associated with the reaction of a fresh pyrite surface as a function of time with the high $\text{H}_2^{18}\text{O}/\text{O}_2$ gaseous mixture. Associated with these spectra are changes principally below 1000 cm^{-1} , assigned to iron oxide species (27) as an intense peak at 862 cm^{-1} having shoulders at $778, 928,$ and 960 cm^{-1} . Relatively minor (and often inconsistent) changes occurred above 1000 cm^{-1} that were not resolved into any kind of band structure. The inset of the figure shows an expansion of the region between 1000 and 1350 cm^{-1} to emphasize the lack of significant change in this spectral region.

Figure 3 displays spectra associated with the changes that occur during the exposure of pyrite to the low $\text{H}_2^{16}\text{O}_2/\text{O}_2$ concentration mixture. The changes in the region above 1100 cm^{-1} are significantly more intense than were observed in the previous high $\text{H}_2^{16}\text{O}_2/\text{O}_2$ experiments. The band between 1100 and 1200 cm^{-1} has a maximum at 1160 cm^{-1} with a shoulder at 1185 cm^{-1} . A broad band of relatively low intensity is located above 1200 cm^{-1} (centered around 1275 cm^{-1}). Assignment of bands in $\text{H}_2\text{O}/\text{O}_2$ -mixture experiments is listed in Table 2 (assignments of observed absorptions are within a range of $\pm 5\%$ of the calculated value). Based on the results

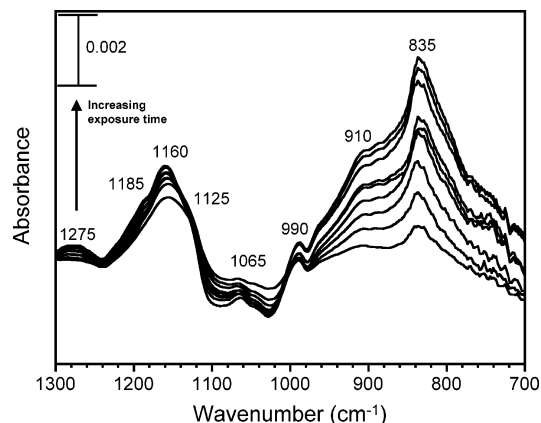


FIGURE 3. Spectra recorded as a function of time (up to 240 min) of pyrite exposed to a low-concentration $\text{H}_2^{16}\text{O}/\text{O}_2$ gaseous mixture (see Experimental Methods for specific conditions).

TABLE 2. Observed Frequencies from $\text{H}_2\text{O}/\text{O}_2$ -mixture Experiments and Assignments Based on Calculations^a

obsd freq	assignt (based on calculations in Table 1)
Low $\text{H}_2^{16}\text{O}/\text{O}_2$ mixture	
990	a, c
1065	a, b
1125	a, b, H-bonded
1160	a, b, d
1185	a, b, d
1275 (broad)	b
$\text{H}_2^{18}\text{O}/\text{O}_2$ mixture	
1000	b, c
1065	a, c, d
1085	a, c
1124	b, d
1158	a, b, d

^a a, b, c, d: refer to structures so labeled in Figure 1.

of theoretical calculations performed by Paul et al. (28) and other literature (29–31), these absorptions can be assigned to bisulfate (HSO_4^-) and/or sulfate (SO_4^{2-}) coordinated to the surface. The existence of a broad mode in our spectra above 1200 cm^{-1} is a signature mode of bisulfate. Simple linear regression analysis of the experimental versus theoretical IR frequencies for the low $\text{H}_2^{16}\text{O}_2/\text{O}_2$ concentration mixture suggests that bisulfate could be coordinated in either a monodentate or bidentate bridging structure. Sulfate in either bidentate or monodentate configuration (see Figure 1) does not include modes above 1200 cm^{-1} . The calculation, however, cannot resolve the binding configuration of the bisulfate species with certainty.

This conclusion, based on the computational analysis of bisulfate [vibrations at 1188 and 1204 cm^{-1} (28)] and sulfate on an iron oxide surface, is consistent with prior literature detailing experimental studies of bisulfate and sulfate on metal oxide surfaces. In prior work by Hug, for example, bisulfate on hematite was associated with an absorption near 1200 cm^{-1} (31) as well as a mode at 1051 cm^{-1} . Additional research by Persson and Lövgren determined that bisulfate, HSO_4^- , was associated with absorptions at 1210 and 1045 cm^{-1} (30). The present results also have a minor absorption at approximately 1065 cm^{-1} , which is in the vicinity of the mid- 1000 cm^{-1} bisulfate absorption band associated with our calculations. However, sulfate species also absorb in the region of $1100\text{--}1300\text{ cm}^{-1}$ (28, 29), and the presence of sulfate in addition to bisulfate cannot be ruled out; coexistence of bisulfate and sulfate on the pyrite surface is likely.

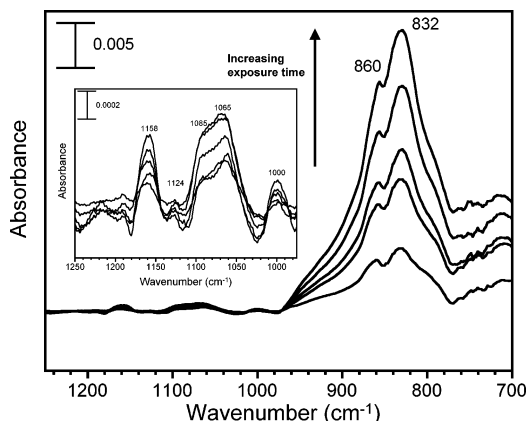


FIGURE 4. Spectra recorded as a function of time (up to 270 min) of pyrite exposed to a gaseous mixture of H_2^{18}O and O_2 . The inset shows an expansion of the spectra region between 975 and 1250 cm^{-1} .

The large band below 1000 cm^{-1} has a maximum at 835 cm^{-1} , corresponding to the iron oxyhydroxide species (27). The position of the iron oxide band in this case is identical to that of the oxide band in liquid experiments (1), while the sulfate bands are blue-shifted from 1100 cm^{-1} (the energy position of the free sulfate ion, observed in aqueous experiments at this position) due to the loss of symmetry upon binding to the pyrite surface. The intensity of the sulfate bands is similar to that of the previous experiments (Figure 2), though the relative intensity of the iron oxide band has decreased.

In a complementary experiment, a low-concentration $\text{H}_2^{18}\text{O}/\text{O}_2$ gaseous mixture was flowed over the pyrite surface. The resulting spectra are shown in Figure 4. In these spectra the surface-coordinated sulfur oxyanion positions have red-shifted (relative to the $\text{H}_2^{16}\text{O}/\text{O}_2$ circumstance) to a group of bands, a weak one at 1124 cm^{-1} , one with a maximum at 1065 cm^{-1} and a shoulder at 1085 cm^{-1} , and one at 1000 cm^{-1} . These peaks are in good agreement with our calculated vibrations for bisulfate and sulfate containing ^{18}O (Table 2). In the bisulfate circumstance, for example, our experiments reveal vibrational modes at 1124, 1085, and 1065 cm^{-1} , and calculations show modes at 1125, 1077, and 1052 cm^{-1} , respectively. Under these particular experimental conditions, simple linear regression analysis of the experimental versus theoretical IR frequencies suggests that bisulfate is coordinated in a bidentate bridging structure. The oxide peaks below 1000 cm^{-1} are in positions similar to the H_2^{16}O experiment (here, at 832 cm^{-1} and a shoulder at 860 cm^{-1}). In this experiment the bisulfate bands are not as intense as the iron oxide bands, and this may be due to slight excess in the amount of water vapor in the ^{18}O experiment as compared to the amount of water vapor in the ^{16}O experiment.

Water Vapor Followed by Introduction of $^{16}\text{O}_2$. A fresh sample of pyrite was exposed to H_2^{16}O vapor carried by N_2 gas for 3 h. The results of this portion of the experiment are shown in Figure 5, displaying absorbance spectra as a function of time. Above 1000 cm^{-1} there are changes over the duration of water exposure, and these can be seen in the inset of Figure 5. Very weak absorptions at 1027, 1063, 1124, and 1186 cm^{-1} appear. On the basis of calculations and the literature, these features are attributed to vibrations of bisulfate and/or sulfate (28–31). The spectra are dominated by an intense band at 865 cm^{-1} , with shoulders at 930 and 835 cm^{-1} and a smaller peak at 960 cm^{-1} . These bands are assigned to an iron hydroxide species, with the peak at 865 cm^{-1} specifically assigned to the Fe–O–H bend (27). While the iron oxide peaks continued to increase in intensity throughout the duration of water exposure, the weak

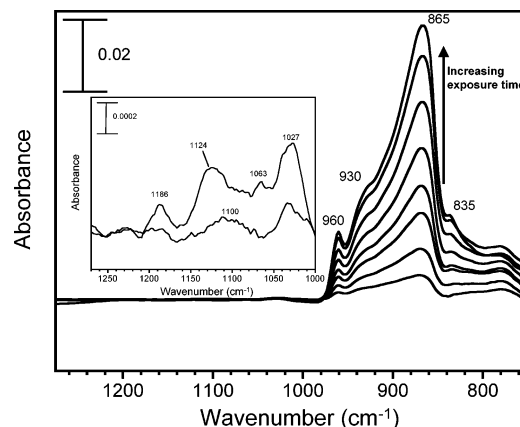


FIGURE 5. Spectra recorded as a function of time (up to 170 min) for the exposure of pyrite particles to H_2^{16}O vapor. The inset shows an expansion of the region from 1000 to 1275 cm^{-1} . For clarity, only two spectra (at $t = 25$ and 120 min) are shown.

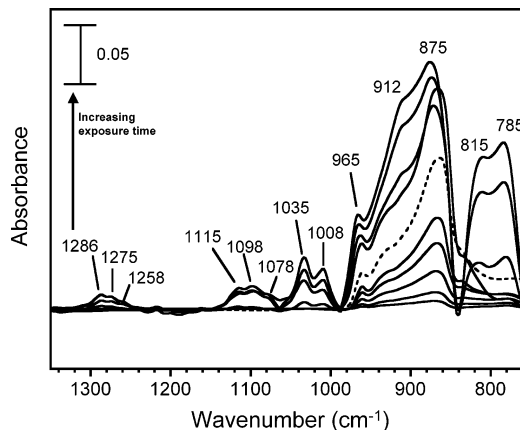


FIGURE 6. Spectra recorded as a function of time for the exposure of pyrite first to H_2^{16}O vapor (carried by N_2 gas, up to 170 min) and then to H_2^{16}O vapor + O_2 gas (up to 180 min). The dotted spectrum indicates the first spectrum recorded after introduction of O_2 gas, and spectra above this line correspond to exposure of pyrite to H_2^{16}O + O_2 gas.

absorptions above 1000 cm^{-1} did not appreciably increase up to the end of the experiment at 3 h of exposure. It is pointed out that prior studies have shown that iron oxides can exhibit peaks above 1000 cm^{-1} (27). However, we attribute peaks in that region in our experiments to sulfur oxyanions, because the growth of these peaks do not show any correlation to the iron oxide-related modes below 1000 cm^{-1} that show a rapid growth with exposure time.

After 3 h, the nitrogen was replaced with $^{16}\text{O}_2$ gas, and the resulting $\text{H}_2\text{O}/\text{O}_2$ mixture was passed over the pyrite sample. Figure 6 exhibits the spectra resulting from the addition of the O_2 to the gaseous H_2O reactant. Also presented for comparison are the data for the H_2O -only exposure experiment. Notably, bands in the sulfate region above 1000 cm^{-1} formed in three groups: (i) features at 1286, 1275, and 1258 cm^{-1} , (ii) peaks at 1115, 1098, and 1078 cm^{-1} , and (iii) peaks at 1035 and 1008 cm^{-1} , with a weak shoulder at 1060 cm^{-1} . These high-wavenumber absorptions (above 1200 cm^{-1}) are all primarily attributed to bisulfate vibrational modes based on the theoretical calculations and literature results (28, 30, 31), though bidentate sulfate species are also reported to absorb in this region (28, 29). The other bands are attributed to sulfate modes, with the 1035 cm^{-1} mode also possibly due to bisulfate. The intense absorption below 1000 cm^{-1} increased considerably with the addition of O_2 , with the appearance of a shoulder at 912 cm^{-1} and two new peaks at

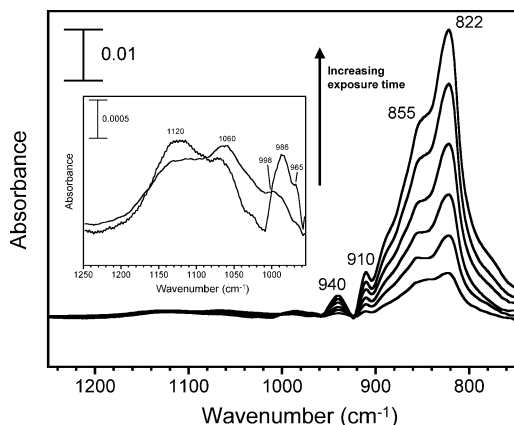


FIGURE 7. Spectra recorded as a function of time (up to 255 min) for the exposure of pyrite particles to H_2^{18}O vapor only (carried by N_2 gas). The inset shows an expansion of the spectra region of $945\text{--}1250\text{ cm}^{-1}$. For clarity only two spectra are shown (at $t = 45$ and 205 min).

815 and 785 cm^{-1} that are thought to be associated with the formation of an iron oxyhydroxide product. All the new peaks, resulting from O_2 addition, increased in intensity with exposure to the mixture of H_2O and O_2 gas. The rate of this increase began to taper off toward the end of the experiment (3 h after introduction of O_2), with the sulfate region showing a plateau in its growth prior to the iron oxide region (primarily below 1000 cm^{-1}).

A companion experiment was performed using H_2^{18}O instead of H_2^{16}O , where $^{16}\text{O}_2$ gas was introduced to the H_2^{18}O reactant stream after the sample was exposed for 255 min to H_2^{18}O vapor alone. The spectra that result from the water exposure alone are shown in Figure 7. Initially, weak absorptions above 950 cm^{-1} appeared that we attribute to surface $\text{S}\text{--}^{18}\text{O}$ vibrations (Figure 7 inset), on the basis of the calculations performed, and these modes grew slowly and mostly plateaued in intensity after 2 h. A relatively weak feature at 940 cm^{-1} increased steadily with time. Again, the most dominant feature in the spectra was the absorption due to iron hydroxide species that occurs below 900 cm^{-1} . The iron hydroxide absorbance exhibited in these spectra has red-shifted from 865 to 820 cm^{-1} relative to the H_2^{16}O vapor experiment. A small peak at 910 cm^{-1} , a shoulder at 855 cm^{-1} , and a weaker shoulder at 885 cm^{-1} also appeared and increased steadily with the main 820 cm^{-1} peak over time. After 4 h, the N_2 carrier was replaced with $^{16}\text{O}_2$. The spectra are shown with the water-only case for comparison in Figure 8. The introduction of O_2 resulted in a significant increase in the intensity of the peak at 820 cm^{-1} , as well as increases in its shoulders and the peak at 910 cm^{-1} . While the increase in these peaks was initially rapid, their growth rate slowed considerably and nearly stopped after 105 min. The most notable changes that occurred were in the region between 950 and 1050 cm^{-1} , shown in the inset of Figure 8, where absorbance increased immediately with the addition of O_2 and continued to slowly increase over time. The features in this particular band were at 1030 , 1008 , 972 , and above 1100 cm^{-1} . These vibrational modes are assigned to $\text{S}\text{--}^{18}\text{O}$ surface bound species based on the similarity to our theoretical calculations of $\text{S}\text{--}^{18}\text{O}$ species, and these modes correspond to an appropriate red-shift of vibrations calculated for $\text{S}\text{--}^{16}\text{O}$ species.

$^{16}\text{O}_2$ Followed by Introduction of Water. Freshly cleaned samples of pyrite were exposed to a flow of pure $^{16}\text{O}_2$ gas for at least 2 h. During the reaction, relatively small changes occurred to the pyrite surface, on the basis of the lack of significant absorbances in the associated HATR-FTIR data (Figure 9). Among these small changes was the formation of

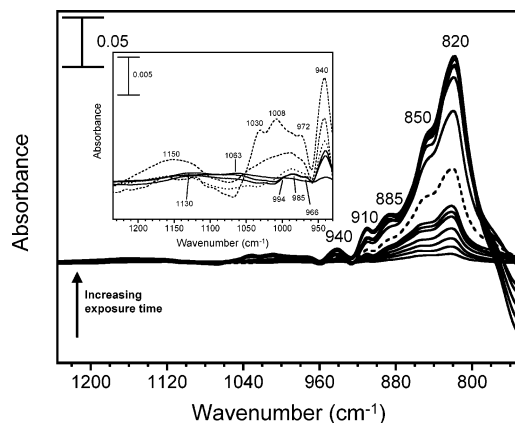


FIGURE 8. Spectra recorded as a function of time of pyrite particles exposed first to H_2^{18}O vapor only (carried by N_2 gas, up to 255 min) then to H_2^{18}O vapor + O_2 gas (up to 105 min). The dotted spectrum indicates the first spectrum taken after introduction of O_2 ; spectra above this line correspond to spectra taken during exposure to H_2^{18}O + O_2 . The inset shows an expansion of the region of $930\text{--}1250\text{ cm}^{-1}$. Solid spectra show absorptions due to H_2^{18}O vapor alone; dotted spectra correspond to H_2^{18}O + O_2 exposure.

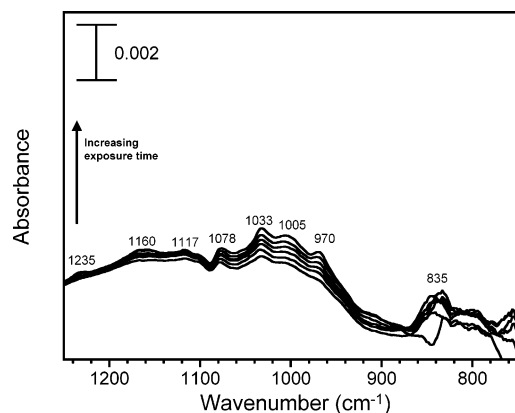


FIGURE 9. Spectra of pyrite particles exposed to pure O_2 gas as a function of time (up to 130 min).

very weak bands in two groups in the region between 900 and 1300 cm^{-1} : (i) features at 1235 , 1160 , and 1117 cm^{-1} and (ii) features at 1078 , 1033 , 1005 , and 970 cm^{-1} . These bands, identified as belonging to $\text{S}\text{--}\text{O}$ vibrations (28, 29, 31) including both bisulfate and sulfate, grew slowly in intensity, and while they did not completely taper off, they did not increase significantly over time. Additionally, an absorption attributed to iron oxide species was observed between 800 and 840 cm^{-1} , but this peak was also very weak (27).

After 2 h, the oxygen flow was stopped and replaced by H_2^{16}O vapor (carried by N_2 gas). Immediately, significant changes occurred, including the growth of intense new bands (Figure 10). The most intense bands were observed below 1000 cm^{-1} , dominated by a peak at 860 cm^{-1} with shoulders at 915 and 935 cm^{-1} and a small peak at 960 cm^{-1} . Another pair of intense bands appeared at 815 and 780 cm^{-1} . These two sets of absorptions are attributed to iron oxide species, specifically iron hydroxide (860 cm^{-1}) and iron oxyhydroxide (815 and 780 cm^{-1}). A third set of absorptions occurred between 1140 and 1000 cm^{-1} , with features at 1110 , 1096 , 1067 , and 1030 cm^{-1} , assigned to sulfate $\text{S}\text{--}\text{O}$ vibrations (28, 29, 31). Above 1200 cm^{-1} there is a broad absorbance that is not resolved into a peak but may be due to bisulfate.

A similar experiment was performed with isotopically labeled water vapor, where the surface was first exposed to pure $^{16}\text{O}_2$ and then to H_2^{18}O vapor carried by N_2 . The results of the O_2 -only portion of the experiment were similar to those

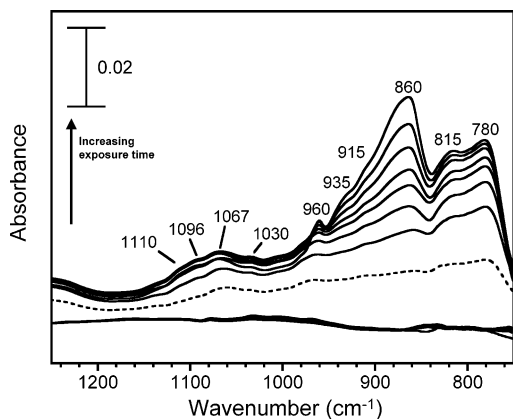


FIGURE 10. Spectra recorded as a function of time of pyrite exposure to O_2 gas only (130 min) and then to $H_2^{16}O$ vapor (carried by N_2 gas, 160 min). The dotted spectrum indicates the first spectrum taken upon introduction of $H_2^{16}O$ vapor. Above the dotted line are subsequent spectra recorded during $H_2^{16}O$ vapor exposure.

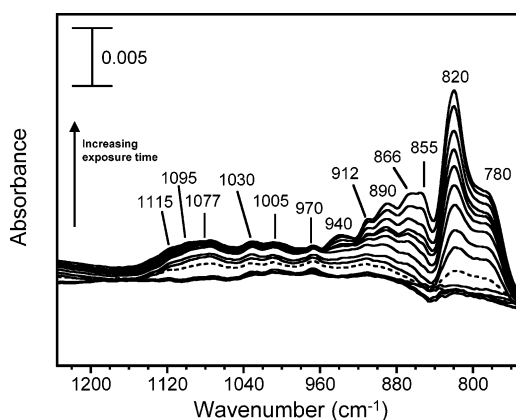


FIGURE 11. Spectra taken as a function of time of the pyrite surface exposed first to O_2 gas alone (130 min) and then to $H_2^{18}O$ vapor (carried by N_2 gas, 175 min). The dotted spectrum indicates the first taken upon introduction of the $H_2^{18}O$ vapor. Spectra above the dotted line were taken during exposure to $H_2^{18}O$ vapor.

described above, but the addition of water vapor containing ^{18}O atoms yielded some changes, shown in Figure 11. In particular, a broad absorption appeared with features at 1115, 1095, and 1077 cm^{-1} , as well as peaks at 1030, 1005, 970, and 940 cm^{-1} , which appeared after the addition of water vapor. These features increased for a period of time and then ceased to grow. These sets of bands are assumed to include S–O vibrations containing both ^{16}O and ^{18}O . The band positions present in this case can be argued not to have shifted relative to the O_2 -then- $H_2^{16}O$ case described above, while others have. Another absorption group with features at 912, 890, and 855 cm^{-1} grew with time, and the dominant peak at 820 cm^{-1} (with a shoulder at 780 cm^{-1}) increased steadily (assigned as the iron hydroxide peak, red-shifted from the ^{16}O counterpart). The intensity of the hydroxide peak is far greater than that for sulfate peaks, a common theme in these experiments.

Discussion

Experimental results presented in this study support the hypothesis that the origin of oxygen in sulfate formed during the oxidation of pyrite is a strong function of the oxidizing environment. In short, pyrite oxidation with gaseous water and oxygen results in sulfate and/or bisulfate product that is comprised of oxygen from both reactants. In contrast, prior studies have shown that sulfate is almost exclusively derived from water-oxygen when pyrite oxidation occurs in solution with dissolved oxygen. The results of the HATR–FTIR

experiments also show that the relative concentration of sulfur oxyanion and iron (oxy)hydroxide surface products vary with reaction conditions. These results suggest that there are competing pathways for the formation of the oxidation products and that the contribution of specific pathways to products is a strong function of the oxidizing environment and the pretreatment of the pyrite surface. In the following, the results will be discussed beginning with the sequential exposures of pyrite to H_2O and O_2 , followed by the results of the exposure to a mixture of H_2O and O_2 to highlight the differences in the effects on the pyrite surface (i.e. differences in surface modification resulting from individual and sequential exposure vs simultaneous exposure).

Exposure of Pyrite to Individual H_2O and O_2 Environments.

When pyrite is exposed to water vapor in a deoxygenated environment, an iron hydroxide product dominates the surface composition. This hydroxide species is shown to be derived from water by isotopic labeling experiments [the hydroxide peak red-shifts when $H_2^{18}O$ is used (Figure 7 vs Figure 5)]. The formation of the water-derived iron hydroxide species is consistent with prior theoretical and experimental research that shows water adsorbs preferentially to iron sites on the pyrite surface (32–38). It is shown by our data that exposure of the pyrite surface to dry O_2 results in a relatively small amount of sulfur oxyanions (Figure 9). We believe that the formation of these species occurs via reaction with monosulfide, based on prior synchrotron-based photoemission research by Kendelewicz et al. that showed the reaction of a pristine pyrite surface with molecular oxygen occurred at sulfur-deficient sites and resulted in sulfur oxyanion production (20). It is suspected that the initial interaction of the O_2 with the surface takes place at iron sites, with dissociation or adsorption of O_2 that leads to interaction with monosulfide defect sites, forming the sulfur oxyanion species observed both in the Kendelewicz study and the present report. Results in this study further suggest that sulfate formation in this instance depends on the history of the sample. For example, in this study, if the O_2 -preexposed pyrite is then exposed to H_2O vapor (no O_2 present), there is a significant amount of sulfate formation. Actually, the increase in sulfate formation in this exposure sequence is greater than what is seen in experiments in which pyrite is exposed to water without preexposure to O_2 . This experimental observation suggests that the O_2 pretreatment modifies the surface in such a way that it can form sulfate more efficiently than when it had been only exposed to H_2O . The isotopic labeling experiments show that in this case the sulfate does contain significant amounts of oxygen atoms derived from O_2 as well as from H_2O . We speculate that the initial exposure to O_2 partially oxidizes the pyrite surface, perhaps leaving some sulfate, but also a fraction of the sulfur more electropositive than the unreacted state (perhaps SO_x , where $x = 1-3$), making it more susceptible to attack by dissociation fragments of chemisorbed H_2O to form sulfate or bisulfate. The relatively small amount of red-shifted sulfate in isotopic labeling experiments would be consistent with this latter fraction. The extent to which the oxygen in the sulfate product is derived from reactant O_2 or H_2O cannot be discerned from our data, except to say that there is a significant partitioning of the oxygen from both these reactants into the sulfur oxyanion product (O_2 -derived portion unshifted, H_2O -derived portion shifted). We can also safely state that the sulfate product in our prior aqueous study is almost exclusively derived by water-oxygen (1). In the present gaseous circumstance, where O_2 reacted with the surface before exposure to H_2O , there is a far greater contribution of oxygen from reactant O_2 to the sulfate product, suggesting that the sequential exposure led to oxidation through a different mechanistic path. Interestingly, these experiments also show that for pyrite oxidation to occur the mineral need only be

sequentially exposed to O₂ and H₂O and a simultaneous exposure is not required. The essentials of such an argument are consistent with the calculations of Rosso et al. in that transfer of electron density to molecular oxygen, which is the terminal electron acceptor, from iron centers results in the withdrawal of density from neighboring sulfur atoms that are then more susceptible to attack by the water reactant which follows (39).

These sequential O₂ and H₂O exposure results also add some insight into our current (and prior) H₂O-alone exposure results. The initial exposure of pyrite to H₂O vapor appears by HATR–FTIR to result in the formation of a minor amount of sulfur oxyanion species. Prior studies based on X-ray photoelectron spectroscopy (XPS) have also suggested that a relatively small amount of sulfate forms on pyrite upon reaction with water (33, 40, 41). In view of our results for the O₂-followed-by-H₂O exposure case mentioned above, it may be that sulfate formation after an initial H₂O vapor exposure in these earlier studies, and in our current study, is due to residual oxygen on the pyrite surface. This contention is consistent with the high-resolution photoelectron data of Kendelewicz et al. (20) that shows that water interacting with a pristine fractured pyrite surface does not lead to sulfate formation.

It is important to point out that we cannot be sure from our HATR–FTIR results whether the sulfur oxyanion production after the sequential exposure to O₂ and H₂O is derived from the monosulfide defect or disulfide group on the pyrite. We suspect that the oxidation of the former group is occurring in these experiments, since prior studies have shown that the initial oxidation of pyrite is restricted to the monosulfide (S²⁻) defect site (41–43).

Exposure of Pyrite to H₂O/O₂ Mixed Environments. Prior research has shown that the exposure of pyrite to gaseous H₂O/O₂ mixtures results in the oxidation of the disulfide group of pyrite in addition to the nonstoichiometric S²⁻ site (41). Comparison of results from our experiments that used two H₂O/O₂ gas mixtures, which differ in the partial pressure of H₂O, show that this oxidation process is highly sensitive to the relative amounts of each gas-phase reactant. Exposure of pyrite to the H₂O/O₂ gas mixture having the higher partial pressure of water vapor yields results that are nearly identical to those of the water-only case. Both experiments are associated with HATR–FTIR spectra that are dominated by water-derived iron hydroxide modes and show little to no significant differences in the sulfate region. Thus, even though molecular oxygen was present during this reaction, only minor amounts of sulfur oxyanion product are formed, and the surface structure is essentially the same as would occur if O₂ were absent. The reaction path in this case would follow that which is associated with H₂O-only conditions. When the mixture with a lower H₂O partial pressure was passed over a clean pyrite surface, however, different results were obtained. In this circumstance, there was little formation of the water-derived iron hydroxide phase that dominates the water-alone experiment. Instead, the dominant Fe phase was oxyhydroxide, similar to that formed in solution (spectral features for this species in the same position, at 835 cm⁻¹ for both gas-phase and aqueous experiments). Also in this scenario there was significant surface-bound sulfur oxyanion formation. On the basis of calculation and comparison of our data to prior studies of sulfur oxyanions on metal oxide surfaces, we believe that the dominant sulfur oxyanion here is bisulfate. This species is perhaps expected to some extent, since the addition of hydroxide, derived from water, is expected to be part of the sulfur oxidation mechanism. Also inferred from our data is that there is a threshold ratio of the reactants that favors sulfur oxyanion and oxyhydroxide formation.

In general, experimental observations suggest that there is competition for surface sites between the reactants, a contention perhaps best exemplified by our observation that more sulfur oxyanion production occurs on pyrite in the H₂O/O₂ vapor stream that contained the lower partial pressure of H₂O. It might be presumed that the water has a significantly higher adsorption energy than molecular oxygen and would increasingly block O₂ access to the surface as its partial pressure increased, consistent with our observations. At the proper ratio, O₂ is able to access reactive Fe sites, facilitating electron transfer and sulfur oxidation.

One of the key questions that need to be answered is how oxygen derived from molecular oxygen is incorporated into the sulfur oxyanion product in our gaseous experiments. In the aqueous circumstance, experimental results show that the incorporation of molecular oxygen (dissolved in solution) into the sulfate product is only a minor reaction channel. As mentioned earlier, this result has been modeled by others (18) in terms of an electrochemical reaction where reduction of O₂ occurs at the cathodic Fe²⁺ site and oxidation at the S-anode results in the formation of sulfate due to the nucleophilic attack of water reactant. Even if a thin water layer exists on the pyrite surface under our high humidity experiments, the electrochemical-based model established on the aqueous oxidation is not very satisfying, given the significant incorporation of oxygen derived from molecular oxygen in the sulfate product. Our gaseous results do, however, suggest that similar to the aqueous circumstance, the initial adsorption site of molecular oxygen is on the Fe-surface site. This experimental observation alone supports the notion that the O₂ reactant does not adsorb and directly attack the sulfur component to form sulfur oxyanion product. Prior experimental/modeling research (44) suggests that the adsorption of molecular O₂ on iron oxide regions of the oxidizing surface is energetically favorable, since the Fe(III)-bearing iron oxide can act as a conduit for electron transfer from Fe(II) at the periphery. It would be presumed in this case that concomitant electron withdrawal from surrounding sulfur would allow attack by water (that may be present as a thin mobile layer) and the insertion of water-derived oxygen into the oxidation product. The presence of a mobile layer on the pyrite surface is supported by recent research by Jerz and Rimstidt (45) who suggest that a ferrous sulfate/sulfuric acid solution film forms on pyrite under moist conditions consistent with our contention from this study that sulfate and bisulfate populate the pyrite surface during the oxidation process. Our isotopic labeling experiments show that these products are not only derived from the water reactant but also the mechanism associated with their formation involves the transfer of a significant amount of oxygen from iron to the sulfur component. We suspect this channel is preceded by the activation of oxygen on Fe sites with subsequent transfer to the sulfur component and/or the transfer of oxygen from iron oxide to the sulfur component. Such processes are reasonable considering prior heterogeneous catalysis literature that shows that iron oxides are effective catalysts for the oxidation of reactants such as H₂S (46) and SO₂ (47) (these types of reactions, however, typically occur at elevated temperatures, >450 K) with added O₂. In our circumstance, only a minor amount of oxidation of pyrite occurs when it is exposed to O₂ alone at room temperature. We suspect that the presence of the adsorbed H₂O layer on pyrite facilitates the oxidation process by contributing O to the sulfur oxyanion product and also by “solvating” the intermediate sulfur oxyanion species and sulfate product. This latter role is most certainly important in the aqueous case where both sulfate and Fe-based product are continuously removed from the pyrite surface allowing the oxidation process to proceed until the pyrite is consumed. Under the gaseous conditions used in the present study, removal of the product from the surface

does not occur, but we presume there is an enhancement of mobility of intermediate and product that facilitates the oxidation process. This statement is also supported by the prior work of Jerz and Rimstidt (45) showing that there are significant dissolution and precipitation reactions occurring on the pyrite surface during oxidation at high humidity. Determining the details of the elementary reactions that lead to the partitioning of oxygen in the oxidation products will have to wait for future experimental and theoretical considerations.

Acknowledgments

D.R.S. and M.A.S. greatly appreciate support from the Department of Energy, Basic Energy Sciences from Grants DEFG029ER14644 and DEFG0296ER14633, respectively. This research also was supported by the Center for Environmental Molecular Science (CEMS) at Stony Brook that is funded by the National Science Foundation (Grant CHE-0221934). Computation was supported in part by the Materials Simulation Center, a Penn-State MRSEC and MRI facility.

Literature Cited

- Usher, C. R.; Cleveland, C. A., Jr.; Strongin, D. R.; Schoonen, M. A. A. Origin of oxygen in sulfate during pyrite oxidation with water and dissolved oxygen: An in situ HATR-IR isotope study. *Environ. Sci. Technol.* **2004**, *38*, 5604–5606.
- Singer, P. C.; Stumm, W. Acidic mine drainage: The rate-determining step. *Science* **1970**, *167*, 1121–1123.
- Hiskey, J. B.; Schlitt, W. J. In *Interfacing technologies in solution mining, proceedings of the 2nd SME-SPE international solution mining symposium*, Denver, CO; Hiskey, J. B., Schlitt, W. J., Eds.; American Institute of Mining, Metallurgical and Petroleum Engineers: New York, 1982; pp 55–74.
- Lowson, R. T. Aqueous oxidation of pyrite by molecular oxygen. *Chem. Rev.* **1982**, *82*, 461–497.
- Alpers, C. N.; Blowes, D. W. *Environmental geochemistry of sulfide oxidation*; American Chemical Society: Washington, D.C., 1994.
- Jambor, J. L.; Blowes, D. W. Mineralogical Association of Canada Short Course 22, 1994.
- Evangelou, V. P. *Pyrite oxidation and its control*; CRC Press: Boca Raton, FL, 1995.
- Evangelou, V. P.; Zhang, Y. L. A review: Pyrite oxidation mechanisms and acid mine drainage prevention. *Crit. Rev. Environ. Sci. Technol.* **1995**, *25*, 141–199.
- Gray, N. F. Field assessment of acid mine drainage contamination in surface and ground water. *Environ. Geol.* **1996**, *27*, 358–361.
- Banks, D.; Younger, P. L.; Arnesen, R.-T.; Iversen, E. R.; Banks, S. B. Mine-water chemistry: The good, the bad, and the ugly. *Environ. Geol.* **1997**, *32*, 157–173.
- Pain, D. J.; Sanchez, A.; Meharg, A. A. The Donana ecological disaster: Contamination of a world heritage estuarine marsh ecosystem with acidified pyrite mine waste. *Sci. Total Environ.* **1998**, *222*, 45–54.
- Nordstrom, D. K.; Alpers, C. N. In *The environmental geochemistry of mineral deposits*; Plumlee, G. S., Logsdon, M. J., Eds.; Society of Economic Geologists: Littleton, CO, 1999; pp 133–160.
- Plumlee, G. S.; Logsdon, M. J. In *Reviews in economic geology*; Society of Economic Geologists: Littleton, CO, 1999; Vol. 6A.
- Abd El-Halim, A. M.; Alonso-Vante, N.; Tributsch, H. Iron/sulfur center mediated photoinduced charge transfer at (100) oriented pyrite surfaces. *J. Electroanal. Chem.* **1995**, *399*, 39–39.
- Bailey, L. K.; Peters, E. Decomposition of pyrite in acids by pressure leaching and anodization: The case for an electrochemical mechanism. *Can. Metall. Q.* **1976**, *15*, 333–344.
- Taylor, B. E.; Wheeler, M. C.; Nordstrom, D. K. Stable isotope geochemistry of acid mine drainage: Experimental oxidation of pyrite. *Geochim. Cosmochim. Acta* **1984**, *48*, 2669–2678.
- Reedy, B. J.; Beattie, J. K.; Lowson, R. T. A vibrational spectroscopic ¹⁸O tracer study of pyrite oxidation. *Geochim. Cosmochim. Acta* **1991**, *55*, 1609–1614.
- Rimstidt, J. D.; Vaughan, D. J. Pyrite oxidation: a state-of-the-art assessment of the reaction mechanism. *Geochim. Cosmochim. Acta* **2003**, *67*, 873–880.
- Schoonen, M.; Elsetinow, A.; Borda, M.; Strongin, D. Effect of temperature and illumination on pyrite oxidation between pH 2 and 6. *Geochem. Trans.* **2000**, *4*.
- Kendelewicz, T.; Doyle, C. S.; Bostick, B. C.; Brown, G. E., Jr. Initial oxidation of fractured surfaces of FeS₂(100) by molecular oxygen, water vapor, and air. *Surf. Sci.* **2004**, *558*, 80–88.
- Frisch, M. J.; Trucks, G. W.; Schlegel, H. B.; Scuseria, G. E.; Robb, M. A.; Cheeseman, J. R.; Montgomery, J. J. A.; Vreven, T.; Kudin, K. N.; Burant, J. C.; Millam, J. M.; Iyengar, S. S.; Tomasi, J.; Barone, V.; Mennucci, B.; Cossi, M.; Scalmani, G.; Rega, N.; Petersson, G. A.; Nakatsuji, H.; Hada, M.; Ehara, M.; Toyota, K.; Fukuda, R.; Hasegawa, J.; Ishida, M.; Nakajima, T.; Honda, Y.; Kitao, O.; Nakai, H.; Klene, M.; Li, X.; Knox, J. E.; Hratchian, H. P.; Cross, J. B.; Bakken, V.; Adamo, C.; Jaramillo, J.; Gomperts, R.; Stratmann, R. E.; Yazyev, O.; Austin, A. J.; Cammi, R.; Pomelli, C.; Ochterski, J. W.; Ayala, P. Y.; Morokuma, K.; Voth, G. A.; Salvador, P.; Dannenberg, J. J.; Zakrzewski, V. G.; Dapprich, S.; Daniels, A. D.; Strain, M. C.; Farkas, O.; Malick, D. K.; Rabuck, A. D.; Raghavachari, K.; Foresman, J. B.; Ortiz, J. V.; Cui, Q.; Baboul, A. G.; Clifford, S.; Cioslowski, J.; Stefanov, B. B.; Liu, G.; Liashenko, A.; Piskorz, P.; Komaromi, I.; Martin, R. L.; Fox, D. J.; Keith, T.; Al-Laham, M. A.; Peng, C. Y.; Nanayakkara, A.; Challacombe, M.; Gill, P. M. W.; Johnson, B.; Chen, W.; Wong, M. W.; Gonzalez, C.; Pople, J. A. *Gaussian 03*, Revisions B.05 and C.01; Gaussian, Inc.: Wallingford, CT, 2004.
- Becke, A. D. Density-functional thermochemistry. 3. The role of exact exchange. *J. Chem. Phys.* **1993**, *98*, 5648–5652.
- Stephens, P. J.; Devlin, F. J.; Chabalowski, C. F.; Frisch, M. J. Ab initio calculation of vibrational absorption and circular dichroism spectra using density functional force fields. *J. Phys. Chem.* **1994**, *98*, 11623–11627.
- Lee, C. T.; Yang, W. T.; Parr, R. G. Development of the Colle-Salvetti correlation-energy formula into a functional of the electron density. *Phys. Rev. B* **1988**, *37*, 785–789.
- Wong, M. W. Vibrational frequency prediction using density functional theory. *Chem. Phys. Lett.* **1996**, *256*, 391–399.
- Foresman, J. B.; Frisch, E. *Exploring chemistry with electronic structure methods*, 2nd ed.; Gaussian, Inc.: Pittsburgh, PA, 1996.
- Ishikawa, T.; Cai, W. Y.; Kandori, K. Characterization of the thermal decomposition products of δ-FeOOH by Fourier transform infrared spectroscopy and N₂ adsorption. *J. Chem. Soc., Faraday Trans.* **1992**, *88*, 1173–1177.
- Paul, K. W.; Borda, M. J.; Kubicki, J. D.; Sparks, D. L. The effect of dehydration on sulfate coordination and speciation at the Fe-(hydr)oxide-water interface: A molecular orbital/density functional theory and Fourier transform infrared spectroscopic investigation. *Langmuir*, accepted for publication, 2005.
- Nakamoto, K. *Infrared and Raman spectra of inorganic and coordination compounds*; 3rd ed.; John Wiley and Sons: New York, 1978.
- Persson, P.; Lövgren, L. Potentiometric and spectroscopic studies of sulfate complexation at the goethite-water interface. *Geochim. Cosmochim. Acta* **1996**, *60*, 2789–2799.
- Hug, S. J. In situ Fourier transform infrared measurements of sulfate adsorption on hematite in aqueous solutions. *J. Colloid Interface Sci.* **1997**, *188*, 415–422.
- Knipe, S. W.; Mycroft, J. R.; Pratt, A. R.; Nesbitt, H. W.; Bancroft, G. M. X-ray photoelectron spectroscopic study of water adsorption on iron sulphide minerals. *Geochim. Cosmochim. Acta* **1995**, *59*, 1079–1090.
- Guevremont, J. M.; Strongin, D. R.; Schoonen, M. A. A. Effects of surface imperfections on the binding of CH₃OH and H₂O on FeS₂(100): Using adsorbed Xe as a probe of mineral surface structure. *Surf. Sci.* **1997**, *391*, 109–124.
- Rosso, K. M.; Becker, U.; Hochella, M. F., Jr. The interaction of pyrite {100} surfaces with O₂ and H₂O: Fundamental oxidation mechanisms. *Am. Mineral.* **1999**, *84*, 1549–1561.
- de Leeuw, N. H.; Parker, S. C.; Sithole, H. M.; Ngoepe, P. E. Modeling the surface structure and reactivity of pyrite: Introducing a potential model for FeS₂. *J. Phys. Chem. B* **2000**, *104*, 7969–7976.
- Becker, U.; Rosso, K. M.; Hochella, M. F., Jr. The proximity effect on semiconducting mineral surfaces: A new aspect of mineral surface reactivity and surface complexation theory. *Geochim. Cosmochim. Acta* **2001**, *65*, 2641–2649.
- Stirling, A.; Bernasconi, M.; Parrinello, M. Ab initio simulation of water interaction with the (100) surface of pyrite. *J. Chem. Phys.* **2003**, *118*, 8917–8926.
- Philpott, M. R.; Goliney, I. Y. Molecular dynamics simulation of water in a contact with an iron pyrite FeS₂ surface. *J. Chem. Phys.* **2004**, *120*, 1943–1950.
- Rosso, K. M.; Becker, U.; Hochella, M. F., Jr. Atomically resolved electronic structure of pyrite {100} surfaces: An experimental and theoretical investigation with implications for reactivity. *Am. Mineral.* **1999**, *84*, 1535–1548.

- (40) Guevremont, J. M.; Elsetinow, A. R.; Strongin, D. R.; Bebie, J.; Schoonen, M. A. A. Structure sensitivity of pyrite oxidation: Comparison of the (100) and (111) planes. *Am. Mineral.* **1998**, *83*, 1353–1356.
- (41) Guevremont, J. M.; Bebie, J.; Elsetinow, A. R.; Strongin, D. R.; Schoonen, M. A. A. Reactivity of the (100) plane of pyrite in oxidizing gaseous and aqueous environments: Effects of surface imperfections. *Environ. Sci. Technol.* **1998**, *32*, 3743–3748.
- (42) Schaufuss, A. G.; Nesbitt, H. W.; Kartio, I.; Laajalehto, K.; Bancroft, G. M.; Szargan, R. Incipient oxidation of fractured pyrite surfaces in air. *J. Electron Spectrosc. Relat. Phenom.* **1998**, *96*, 69–82.
- (43) Andersson, K.; Nyberg, M.; Ogasawara, H.; Nordlund, D.; Kendelewicz, T.; Doyle, C. S.; Brown, G. E., Jr.; Pettersson, L. G. M.; Nilsson, A. Experimental and theoretical characterization of the structure of defects at the pyrite FeS₂(100) surface. *Phys. Rev. B: Condens. Matter Mater. Phys.* **2004**, *70*, 195404/195401–195404/195405.
- (44) Eggleston, C. M.; Ehrhardt, J.-J.; Stumm, W. Surface structural controls on pyrite oxidation kinetics: An XPS–UPS, STM, and modeling study. *Am. Mineral.* **1996**, *81*, 10361056.
- (45) Jerz, J. K.; Rimstidt, J. D. Pyrite oxidation in moist air. *Geochim. Cosmochim. Acta* **2004**, *68*, 701–714.
- (46) Keller, N.; Pham-Huu, C.; Crouzet, C.; Ledoux, M. J.; Savin-Poncet, S.; Nougayrede, J.-B.; Bousquet, J. Direct oxidation of H₂S into S. New catalysts and processes based on SiC support. *Catal. Today* **1999**, *53*, 535–542.
- (47) Dunn, J. P.; Stenger, H. G., Jr.; Wachs, I. E. Oxidation of SO₂ over supported metal oxide catalysts. *J. Catal.* **1999**, *181*, 233–243.

Received for review April 7, 2005. Revised manuscript received July 1, 2005. Accepted July 13, 2005.

ES0506657